Numerical Simulation of Land-Breeze-Induced Snowbands Along the Western Shore of Lake Michigan

ROBERT J. BALLENTINE

Atmospheric Sciences, University of Wisconsin–Milwaukee, Milwaukee 53201

(Manuscript received 28 January 1982, in final form 4 June 1982)

ABSTRACT

Case studies are presented which describe a type of lake-effect snowband which forms along the western shore of Lake Michigan when a cold anticyclone to the north sets up an easterly gradient over the lake. Numerical simulations indicate that the snowband coincides with a narrow band of upward motion which results from the convergence of easterly winds over the lake and north to northwesterly winds over land. The northerly winds are part of a land breeze circulation which forms when cold air is heated by the relatively warm lake surface.

Initial data for model simulations are obtained by objective analysis of upper-air data from the eight upper-air stations closest to Lake Michigan at six levels in the lower troposphere. Model results show that a pool of cold air over the lake up to about 850 mb favors rapid growth of the planetary boundary layer over the western half of the lake, and that latent heat release plays an important role in intensifying the land breeze circulation.

1. Introduction

The snow that forms when cold air flows across the Great Lakes in late fall and winter tends to fall over adjacent land areas in one or more narrow bands. In the case of strong northerly or northwesterly flow over Lake Michigan, the snowband may extend from 50 to 100 km inland over portions of northern Indiana or southwestern Michigan and produce its heaviest snowfall along an axis approximately parallel to the low-level wind direction. Because of the long fetch across open water, intense convergence along the rim of the snowband, and persistence of the large-scale flow pattern, this type of snowband has been responsible for very large accumulations of snow at locations such as South Bend, Indiana.

With northeasterly or easterly flow, a narrow snowband may form along the western shore of the lake. In this case the heaviest snowfall is observed near the lakeshore and the orientation of the snowband is more nearly perpendicular to the low-level flow across the lake and approximately parallel to the shoreline. Snowfall rates tend to be much smaller with this type of snowband than with the spectacular South Bend snowbursts. However, the mesoscale circulation responsible for the western shore snowbands is likely to persist for many hours resulting in slippery roads and reduced visibility in heavily populated sections of Milwaukee or Chicago. Although typical maximum snowfall accumulations are only 3–5 inches, the impact of the western shore snowband is probably as great as the South Bend-type storms, since more people are affected by the snow.

Passarelli and Braham (1981) investigated shoreline parallel snowbands near Lake Michigan. On the basis of aircraft and radar observations, they concluded that these snowbands are manifestations of vertical air motions generated at a very sharp land-breeze-induced confluence line over the lake. Their case studies illustrated the importance of the shallow land breeze in organizing the low-level convergence and convective motions. The role of the land breeze in producing a band of enhanced precipitation parallel to the coastline was emphasized by Ballentine (1980). He concluded, from experiments with a three-dimensional numerical model, that the low-level convergence in a New England coastal front resulted primarily from a land breeze circulation which develops when heating of air over the ocean produces a solenoidal field in a vertical plane perpendicular to the coast. The author observed that the intensity of this mesoscale circulation is proportional to the air-sea temperature difference for waters just off the New England coast.

In this investigation the mesoscale model described by Ballentine (1980) is adapted to the geography of Lake Michigan for the purpose of simulating the shoreline-parallel snowbands. The primary object is to examine the effect of the larger scale initial conditions and the role of latent heat release on the location and intensity of the snowband circulation.

2. Case studies

Synoptic conditions which favor the development of shoreline-parallel snowbands along the western

0027-0644/82/111544-10$06.50

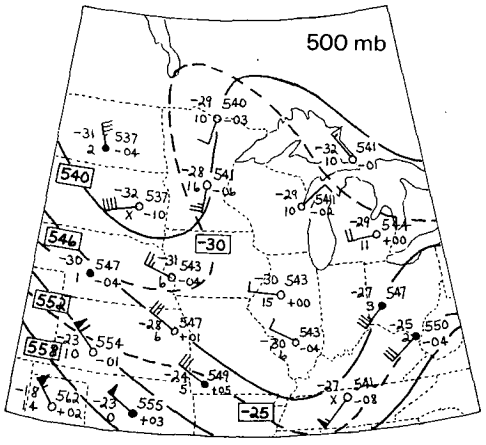

FIG. 1. Reproduction of a portion of the NMC 500 mb analysis for 1200 GMT 4 January 1980.

shore of Lake Michigan are illustrated in two case studies.

a. 4 January 1980

A portion of the NMC 500 mb analysis for 1200 GMT is shown in Fig. 1. A weak trough extends from the eastern Dakotas to extreme western Kentucky. Lake Michigan is beneath the downstream ridge axis. The flow at 850 mb (not shown) is quite weak over the Great Lakes. An important feature is a pocket of relatively cold air at 850 mb centered over Lake Michigan. The Green Bay sounding at 1200 GMT shows the temperature at 861 mb to be −16°C, while temperatures at the surrounding stations are −12°C or warmer. Since the Lake Michigan water surface temperature is ~20°C warmer than the overlying air near 850 mb, the lower portion of the atmosphere is absolutely unstable over the lake.

At the surface at 1200 GMT, a 1012 mb low was centered over North Dakota and light snow was falling over most of the upper Mississippi Valley. A cold anticyclone was situated to the northeast of Lake Michigan (Fig. 2a). Winds at most locations were from the east or northeast, but winds at stations along the western shore of the lake were from the northwest deviating almost 180° from the geostrophic wind direction. This wind pattern, with apparent low-level convergence along the western shore, persisted for approximately 12 h. The temperature difference across the lake (compare Milwaukee and Muskegon, for example) suggests that the air warmed only 1 or 2°C as it crossed the lake. However, the dewpoint difference increased from 2 to 8°C between 1200 and 2100 GMT indicating that a considerable amount of moisture evaporated into the air from the lake surface. It is hypothesized that a significant fraction of this moisture condensed in clouds near the western shoreline. Light snow in advance of the North Dakota low spread over most of Wisconsin and Michigan during the day, but water equivalents totaled only a trace to 0.3 mm at most stations away from the lake. Closer to the lake, Milwaukee reported 7.6 cm of snow and the University of Wisconsin–Milwaukee (UWM) recorded 10 cm. On the northwest side of Milwaukee (~10 km from the lake) only about 1 cm of snow fell.

b. 16 December 1980

In contrast to the previous case, moderately strong northwesterly flow with cyclonic curvature characterizes the 500 mb flow pattern (not shown) over the

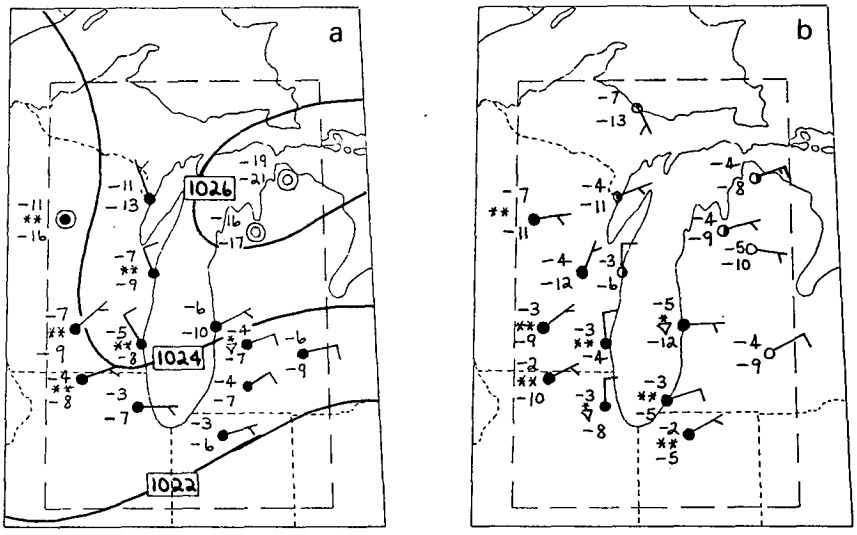

FIG. 2. Surface analyses for 4 January 1980: (a) 1200 GMT (b) 2100 GMT. Solid lines are sea level isobars. Temperatures in °C. For winds full barb is 5 m s^{-1}. The inner (dashed) rectangle indicates the domain of integration for the numerical simulations.

upper Midwest. A strong north-south temperature gradient exists at 850 mb with the axis of the thermal trough aligned directly over Lake Michigan (Fig. 3). Weak cold advection is occurring over the lake to the rear of the sprawling low to the east. At the surface a cold anticyclone over James Bay and a weak cyclone over the southeastern states produce an east-northeasterly gradient over lower Michigan and a weaker easterly gradient over Wisconsin. At 1200 GMT (Fig. 4), there is evidence of a very short wavelength inverted trough over northeastern Wisconsin. This may be the result of heating in the boundary layer over Lake Superior, or it may be due to a subsynoptic-scale wave disturbance aloft. As in the previous case, low-level convergence is apparent along the western shore of Lake Michigan for a period of about 12 h (0600 to 1800 GMT). Scattered light snow showers were reported over both Wisconsin and Michigan, but the only significant accumulations were along the western shoreline, e.g., Milwaukee 5 cm and Sturgeon Bay 7.6 cm.

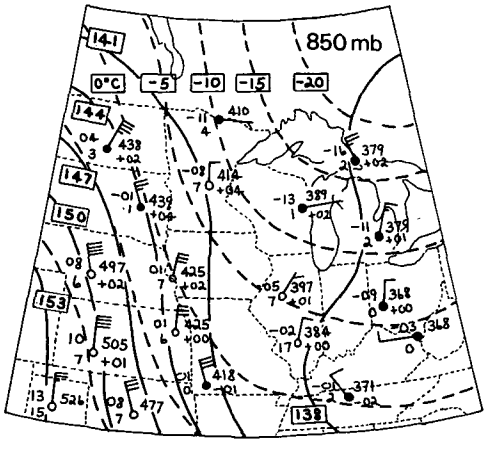

FIG. 3. Reproduction of a portion of the NMC 850 mb analysis for 1200 GMT 16 December 1980.

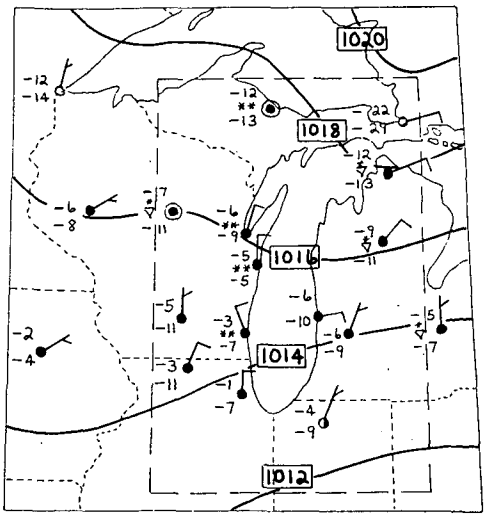

FIG. 4. As in Fig. 2a except for 16 December 1980.

3. Numerical model

The original version of the mesoscale model is described by Ballentine (1980). Improvements and adaptations to Lake Michigan are presented below.

a. Grid

The domain of integration covers Lake Michigan and portions of surrounding states. The horizontal grid size is one-eighth of a degree of longitude (~10 km) in the x (east-west) direction and one-sixth of a degree of latitude in the y (north-south) direction. There are 49 grid points in the x-direction and 41 points in the y-direction. The Lake Michigan shoreline is approximated in the model by connecting appropriate grid points. This results in a reasonably accurate representation of the lake boundary if Green Bay is ignored.

The vertical coordinate r is given by

$$r = B \ln\left(1 + A\frac{z - E}{H - E}\right), \tag{1}$$

where z is height above sea level, $E = E(x, y)$ is terrain elevation, H is the height of the top of the model (5000 m) and B a constant. Since $A = \exp(1/B) - 1$, the coordinate r increases monotonically from 0 to 1 as z increases from E to H. Since the land surrounding Lake Michigan is fairly flat, especially on the western side of the lake, E is taken to be constant (177 m) over the domain. Vertical velocity $\dot{r}$ and Exner function Π are defined at each of the 13 levels in the model. The prognostic variables u, v, q and θ (a list of symbols appears in the Appendix) are defined as layer averages in each of the 12 layers between the grid levels. The vertical grid arrangement is illustrated in Fig. 5. The fine vertical resolution in the lowest portion of the domain helps provide accurate estimation of the vertical transfer of heat and moisture from the surface into the planetary boundary layer (PBL). The constant B is chosen to ensure that the first model layer above the surface is located within the constant stress layer.

b. Model equations

The prediction equations for u, v, q and θ are given in Ballentine (1980). The upstream finite-difference method is used to obtain approximate solutions.

The remaining equations are

$$p = \rho RT, \tag{2}$$

$$\Pi = c_p\left(\frac{p}{1000}\right)^{R/c_p}, \tag{3}$$

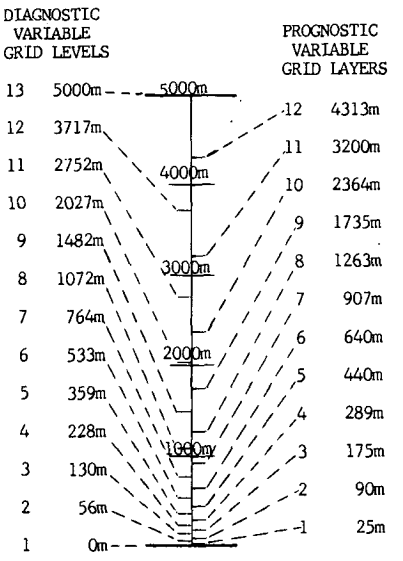

FIG. 5. Vertical grid arrangement.

$$c_pT = \theta\Pi, \tag{4}$$

$$\frac{\partial \Pi}{\partial r} = -\frac{g}{D\theta}, \tag{5}$$

$$\nabla_3 \cdot \mathbf{V} + \frac{d \ln\rho}{dt} = 0, \tag{6}$$

where

$$\frac{d}{dt} = \frac{\partial}{\partial t} + \mathbf{V}_h \cdot \nabla_2 + \dot{r}\frac{\partial}{\partial r}.$$

c. Upper boundary condition

In the original version of the model, the upper boundary was assumed to be a free surface whose initial height above sea level was $H = 2500$ m. Pressure was specified at $z = H$ as a function of time and space according to the propagation of the 700 mb wave disturbance during a case study, and the model atmosphere was assumed hydrostatic. An equation for the vertical velocity $\dot{r}$ was derived from the incompressible continuity equation. In the present model the upper boundary is a rigid lid at $H = 5000$ m above sea level. The hydrostatic approximation is still made, but the atmosphere is no longer assumed to be incompressible.

To derive an equation for vertical velocity, we begin by combining Eqs. (2), (3) and (4) to obtain

$$\frac{d \ln\rho}{dt} = \frac{c_v}{R}\frac{d \ln\Pi}{dt} - \frac{d \ln\theta}{dt}.$$

Then, Eq. (6) may be written in the form

$$\nabla_3 \cdot \mathbf{V} + \frac{c_v}{R}\frac{1}{\Pi}\frac{d\Pi}{dt} - \frac{1}{\theta}\frac{d\theta}{dt} = 0. \tag{7}$$

To eliminate $d\Pi/dt$, we multiply (7) by p/Π and obtain, after some manipulation,

$$\nabla_3 \cdot \left(\frac{p}{\Pi}\mathbf{V}\right) = -\frac{c_v}{R}\frac{p}{\Pi^2}\frac{\partial \Pi}{\partial t} + \frac{p}{\theta\Pi}\frac{d\theta}{dt}. \tag{8}$$

Next, the hydrostatic equation (5) is integrated from level r to the top of the model $r = 1$ ($z = H$) giving

$$\left.\frac{\partial \Pi}{\partial t}\right|_r = \left.\frac{\partial \Pi}{\partial t}\right|_1 - g\int_r^1 \frac{1}{D\theta^2}\frac{\partial \theta}{\partial t}\,ds = M + N,$$

where

$$M = \left.\frac{\partial \Pi}{\partial t}\right|_1, \tag{9}$$

$$N = -g\int_r^1 \frac{1}{D\theta^2}\frac{\partial \theta}{\partial t}\,ds. \tag{10}$$

Then, Eq. (8) becomes

$$\frac{\partial}{\partial z}\left(\frac{p}{\Pi}w\right) = -\frac{\partial}{\partial x}\left(\frac{p}{\Pi}u\right) - \frac{\partial}{\partial y}\left(\frac{p}{\Pi}v\right) - \frac{c_v}{R}\frac{p}{\Pi^2}(M + N) + \frac{p}{\Pi\theta}\frac{d\theta}{dt}. \tag{11}$$

In the case of flat terrain, $\dot{r} = Dw$. Also, $D = \partial r/\partial z$ and it follows from Eq. (1) that $\partial D/\partial r = -D/B$. Using these relationships, (11) may be written in the form

$$\frac{\partial \dot{r}}{\partial r} + b(r)\dot{r} = F(r), \tag{12}$$

where

$$b(r) = \frac{1}{B} - \frac{c_v g}{RD\theta\Pi},$$

$$F(r) = -\frac{\Pi}{p}\left[\frac{\partial}{\partial x}\left(\frac{p}{\Pi}u\right) + \frac{\partial}{\partial y}\left(\frac{p}{\Pi}v\right)\right] + \frac{1}{\theta}\frac{d\theta}{dt} - \frac{c_v}{R\Pi}(M + N). \tag{13}$$

To solve (12) we multiply through by the integrating factor

$$\exp\left[\int_0^r b(s)ds\right],$$

giving

$$\frac{d}{dr}\left\{\dot{r}\exp\left[\int_0^r b\,ds\right]\right\} = F(r)\exp\left[\int_0^r b\,ds\right]. \tag{14}$$

Finally, $\dot{r}$ is computed by integrating (14) upward from the surface applying the lower boundary condition $\dot{r} = 0$ at $r = 0$.

The value of the vertical velocity depends on the forcing terms on the right side of Eq. (13). The first term, representing horizontal mass convergence, normally dominates the other terms. The second term is due to diabatic heating and may become significant in regions of strong latent heat release. The last term involves the integrated heating in the column above (term N) and the pressure tendency at the top of the

model (term M). All terms except M can be evaluated directly from recently computed values of the prognostic variables.

M may be evaluated by integrating (14) from $r = 0$ to $r = 1$ and applying a boundary condition at the top. Application of the lower boundary condition gives

$$\dot{r}(1) = \exp\left[-\int_0^1 bds\right]\int_0^1 F(r)\exp\left[\int_0^r bds\right]dr.$$

One possibility is to assume that the vertical velocity vanishes at the top of the model, i.e., $\dot{r}(1) = 0$. Then

$$0 = \exp\left[-\int_0^1 bds\right] \times \int_0^1 \left\{-\frac{\Pi}{p}\left[\frac{\partial}{\partial x}\left(\frac{p}{\Pi}u\right)+\frac{\partial}{\partial y}\left(\frac{p}{\Pi}v\right)\right] + \frac{1}{\theta}\frac{d\theta}{dt} - \frac{c_v}{R\Pi}(M+N)\right\}\exp\left[\int_0^r bds\right]dr$$

and

$$M = \frac{-\int_0^1 \left\{\frac{\Pi}{p}\left[\frac{\partial}{\partial x}\left(\frac{p}{\Pi}u\right)+\frac{\partial}{\partial y}\left(\frac{p}{\Pi}v\right)\right] - \frac{1}{\theta}\frac{d\theta}{dt} + \frac{c_v N}{R\Pi}\right\}\exp\left[\int_0^r bds\right]dr}{\frac{c_v}{R}\int_0^1 \frac{1}{\Pi}\exp\left[\int_0^r bds\right]dr}. \tag{15}$$

In practice (15) is used to evaluate M at the end of each time step from the prognostic variables. Then, $\dot{r}$ is computed by integrating (14) up from the surface. Eq. (15) also provides the upper boundary condition for pressure (Exner function). The magnitude of M remains quite small during the numerical experiments. Equivalent changes in pressure at the top accumulate up to a few hundredths of a millibar after 12 h of integration. A relatively short time step (36 s) is required because of the propagation of fast-moving waves across the top.

d. *Lateral boundary conditions*

Lateral boundary conditions in the present model are based on the radiation condition proposed by Klemp and Lilly (1978). For the normal velocity component, the object is to minimize reflection from the boundaries of the relatively fast-moving wave modes which can propagate both upstream and downstream. Representative phase velocities are estimated at both inflow and outflow boundaries from recently computed values of the normal velocity at the boundary and first grid point in from the boundary. For example, at the west boundary

$$u - c^* = -\frac{u_t}{u_x}, \tag{16}$$

where u_t and u_x at the boundary are approximated by centered differences one-half grid interval in from the boundary at time level $t - \frac{1}{2}\Delta t$. Then, the value of u at the west boundary is determined by solving

$$\frac{\partial u}{\partial t} + (u - c^*)\frac{\partial u}{\partial x} = 0 \tag{17}$$

at the boundary instead of the east-west equation of motion. At each grid column along the boundary, the vertical average of c^* is computed, as in Klemp and Lilly (1978), instead of the value at each boundary point. The sign of $u - c^*$ is tested to determine if the propagation is *out* of the domain. If not, the value of $u - c^*$ is equated to zero before the vertical averaging. Eq. (17) is solved by the upstream method using values of u at the boundary and the first interior grid point to approximate the spatial derivative.

For specific humidity and tangential velocity component, determination of the boundary value depends on whether the boundary point is an inflow point or an outflow point. At an outflow boundary, boundary values are computed by solving the appropriate governing equation using the upstream method. At an inflow boundary, the upstream method is not stable when interior values are used to approximate the spatial derivative normal to the boundary. Instead, that part of the tendency due to advection (and pressure gradient force and Coriolis force in the case of tangential velocity component) is equated to zero. This means that changes in q and tangential velocity at an inflow boundary are due entirely to vertical diffusion. For potential temperature the part of the tendency due to advection is equated to zero at all lateral boundary points.

This set of boundary conditions is stable and appears to give the most satisfactory results of all the conditions tested in both the two- and three-dimensional versions of the model.

e. *Growth of the PBL*

In the original version of the model, the height of the PBL over the ocean was specified on the basis of available radiosonde data and held fixed in time. In situations where the lower boundary is considerably warmer than the air flowing over it, such as in Lake Michigan snowband cases, it is reasonable to expect the height of the PBL to grow with time. Therefore, in the present model, the height of the PBL is predicted each time step using the method of Deardorff (1974). The growth rate depends primarily on the

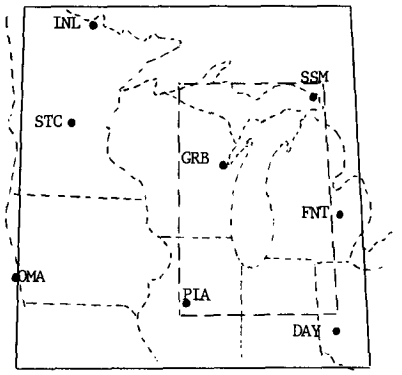

FIG. 6. Horizontal grid and upper-air stations used in initialization. Large rectangle (solid) is boundary of 105 × 61 grid and small rectangle (dashed) is boundary of 49 × 41 grid.

heat flux from the surface and on the magnitude of the mesoscale vertical velocity at the level of the top of the PBL. This results in a positive feedback since the intensity of the mesoscale circulation tends to be greatest where the PBL has grown most rapidly.

Over land, where the PBL is more stable, its height z_B is estimated from the diagnostic equation suggested by Deardorff (1972), i.e.,

$$z_B = \left(\frac{1}{30L} + \frac{f}{0.25u_*}\right)^{-1}.$$

The stability length L and friction velocity u_* are computed each time step from predicted vertical gradients of wind speed and potential temperature in the constant stress layer as in Pielke and Mahrer (1975).

f. Initialization

Since the development of the mesoscale circulation producing the snowbands is likely to depend on the large-scale meteorological fields, it is important to make use of as much synoptic-scale information as possible. In the present model, the pressure at 5000 m and the temperature at 500, 700, 850, 900 and 950 mb and the surface are analyzed objectively to the model grid using radiosonde data from the eight upper-air stations closest to Lake Michigan. The method of Barnes (1964) is used to fit the data to a 105 × 61 grid covering the upper-air stations (Fig. 6), and an analysis to the 49 × 41 grid of the model is extracted from the larger analysis. At each grid column, the hypsometric relation is used to interpolate temperature to each of the layers of the model. Pressure is computed hydrostatically downward from the top, and then the initial wind is computed at all grid points from geostrophic balance. The model variables adjust gradually to the lower surface during the first few hours of integration through the parameterization of boundary layer processes in the model using the method of Pielke and Mahrer (1975).

The initial pressure analyses at 5000 m computed in the numerical simulations from the 1200 GMT data are presented in Fig. 7, and the initial computed surface analyses are shown in Fig. 8. In both the 4 January case and the 16 December case, strong baroclinicity in the lower troposphere results in a reversal of the flow pattern between 5000 m and the surface. For the 4 January case, the computed analysis places the surface high just a little north of its observed position (Fig. 2a), but the easterly gradient over the lake is quite satisfactory. For the 16 December case, there is good general agreement between the observed pressure pattern (Fig. 4) and the computed surface pressure analysis. The latter indicates very little amplitude to the inverted trough over northeastern Wisconsin because this mesoscale disturbance is not resolved from the upper-air data. The large-scale meteorological conditions at 1200 GMT for both case studies appear to be well represented in the model by using data from the eight upper-air stations at six levels.

The initial moisture profile for both simulations reflects the shallow cloud layer extending from about 800 to 1600 m above the surface. The initial relative humidity in the model increases from about 50% near the surface to 100% at cloud base. Above the cloud layer, the relative humidity is ~30% up to the top of the model.

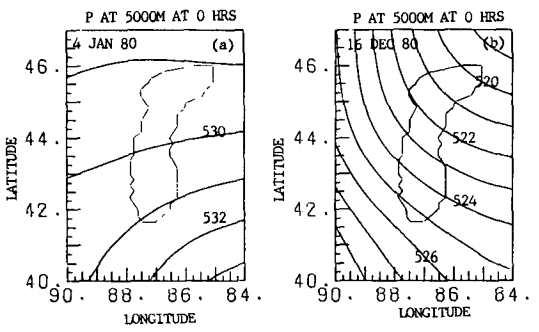

FIG. 7. Initial pressure (mb) computed at top of model for (a) 1200 GMT 4 January 1980 and (b) 1200 GMT 16 December 1980. Contour interval is 1 mb. Thin solid line represents boundary of Lake Michigan.

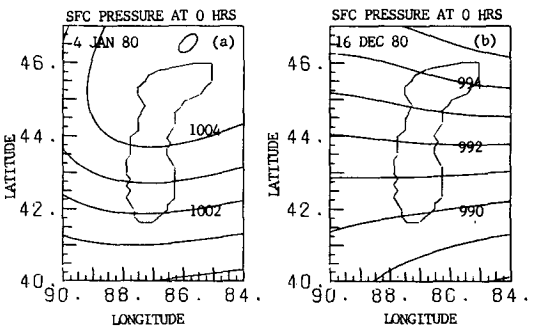

FIG. 8. As in Fig. 7 except at model surface (177 m above sea level).

Some simplifications are made in the specification of conditions at the lower surface in the model. In the 4 January simulation, the land surface temperature is held constant in time at values ranging from −2°C near the southern boundary to −11°C near the northeastern corner of the domain. Along the western shore of the lake, the land temperature ranges from about −3 to −7°C. At grid points over the lake, the surface temperature is held fixed in time at 5°C. The surface roughness length in the model is 10 cm over land and 0.01 cm over the lake.

4. Results

All numerical experiments are integrated out to 12 h from initial conditions at 1200 GMT.

a. 4 January 1980 simulation

1) SURFACE WIND

As the integration proceeds, the u-component at 25 m above the surface gradually becomes more negative over the lake and less negative (positive at a few grid points) over the land closest to the western shoreline. At the same time, the v-component becomes increasingly negative over land near the western shore, but becomes positive over the southwestern portion of the lake. This backing with time of the low-level wind over land is part of the land breeze—a countercurrent superimposed on the large-scale easterly flow—which arises when air over the lake is heated from below. Fig. 9 shows the 25 m wind after 12 h. Only that portion of the domain covering the southern two-thirds of the lake is shown. The length of each vector is proportional to wind speed, and the maximum wind speed over the domain (6 m s^{-1}) is indicated by the number 6 and its vector equivalent in the upper right corner. A distinct line of convergence is evident parallel to and just inland from the western lakeshore where the easterly flow over the lake meets the weaker flow over land which has backed with time to a more northerly direction. No convergence is predicted in the vicinity of the eastern shoreline. The wind predicted by the model is in general agreement with observations (Fig. 2) except that the observed wind at stations near the western shore has backed even more with time to northwesterly.

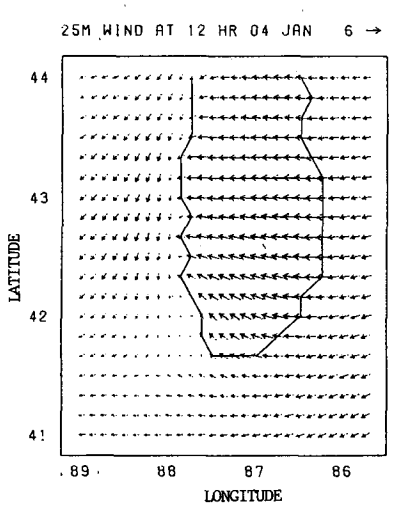

FIG. 9. Horizontal wind at 25 m above surface predicted by model after 12 h of integration for 4 January 1980 simulation. Number at upper right indicates maximum wind speed (m s^{-1}). Thin solid line represents lake boundary.

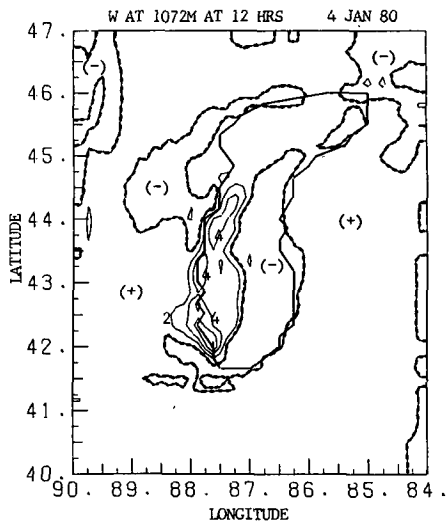

FIG. 10. Vertical velocity w (cm s^{-1}) at 1072 m after 12 h for 4 January 1980 simulation with latent heat included. Contour interval is 2 cm s^{-1}. Bold dashed curve is zero vertical velocity contour.

2) VERTICAL VELOCITY

The vertical velocity at 1072 m above the surface after 12 h (Fig. 10) reflects the line of low-level convergence along the western shoreline. The strongest upward motion, outlined by the 4 cm s^{-1} contour, extends from near Chicago north-northeastward to a point over the lake east of Green Bay. The greatest value of w is about 9 cm s^{-1} and is found near the southern end of the band. The magnitude of the upward motion, which is a measure of the intensity of the mesoscale circulation, increases most rapidly between 3 and 6 h of integration, but changes little between 9 and 12 h.

3) MOISTURE AND PRECIPITATION

The greatest changes in low-level specific humidity occur near the western shore of the lake. At the grid point closest to Milwaukee at 25 m above the surface, the value increases from 2.1 g kg^{-1} at 3 h to nearly 3.1 g kg^{-1} at 12 h. This is partly because of evaporation from the lake surface and partly due to the evaporation of precipitation falling from the column

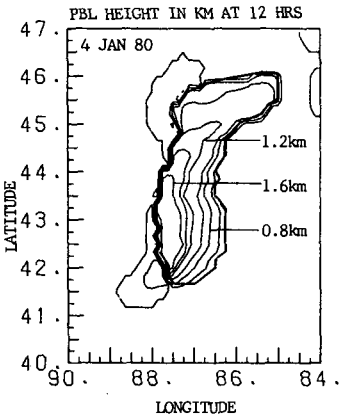

FIG. 11. Predicted height of the planetary bounday layer after 12 h of integration for 4 January 1980 simulation with latent heat included. Contour interval is 0.2 km.

above. Precipitation in the model is computed using the saturation adjustment procedure of Asai (1965). When supersaturation occurs at a grid point, condensation takes place and the liquid water is assumed to fall immediately to the next grid point below where some or all of it may evaporate. Precipitation falls out of the column only if saturation exists at all grid points between the surface and the top of the cloud layer. Precipitation is heaviest where moisture convergence is greatest and where a saturated column is cooled the most because of mesoscale ascent. At 12 h, the only precipitation predicted by the model occurs along the band of upward motion near the western shoreline. The greatest accumulation is about 3 mm near the southern end of the band, corresponding to ~2 inches of low-density, lake-effect snowfall. This is somewhat less than observed in the case study, and the location of the predicted maximum is south of the observed maximum over land. It is possible that some of the heaviest snowfall associated with the real snowband fell just offshore and was not observed.

4) TEMPERATURE

The temperatures predicted by the model at 25 m above the surface agree very well with the observed surface temperatures in the case study. At the grid point closest to Milwaukee, the temperature increases from −4.4°C at 3 h to −2.9°C at 12 h.

5) PBL HEIGHT

The predicted height of the planetary boundary layer over the lake increases steadily during the first 9 h of integration reaching a maximum height of about 1600 m. Little change is predicted after 9 h. At 12 h (Fig. 11), the height is greatest over the western half of the lake where mesoscale upward motion contributes to the growth rate of the PBL.

6) ROLE OF LATENT HEAT RELEASE

A second run of the 4 January simulation was conducted, identical to the first, except that no latent heat was released. A line of convergence near the western shoreline is apparent in the 25 m wind field (Fig. 12), but it is significantly weaker than in the first experiment (Fig. 9). The main difference is that the winds over eastern Wisconsin have a larger easterly component (weaker countercurrent) when latent heat is *not* released. This suggests that the heating due to condensation plays an important role in the intensification of the mesoscale land breeze circulation associated with the shoreline parallel snowbands. The maximum vertical velocity at 12 h was about 5 cm s^{-1} in the second run (compared with 9 cm s^{-1} in the first) and this occurs at a lower level indicating a shallower circulation. Also, the maximum predicted

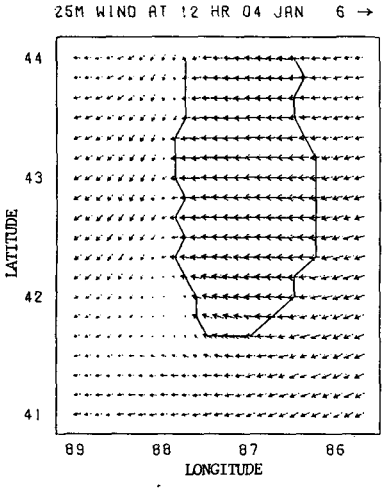

FIG. 12. As in Fig. 9 except for run in which latent heat release is *not* included.

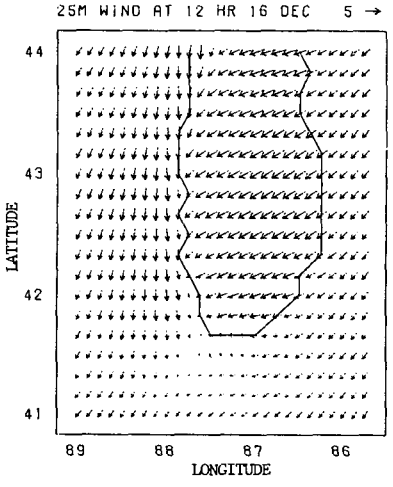

FIG. 13. As in Fig. 9 except for 16 December 1980 simulation.

height of the PBL was about 300 m lower in the run without latent heat release.

b. 16 December 1980 simulation

Since the large-scale, low-level easterly flow is somewhat weaker in the 16 December case, especially over the southwestern portion of the domain, the location of the line of convergence at 25 m above the surface at 12 h (Fig. 13) is predicted to be about 10 km farther east (farther offshore) than in the 4 January simulation. Also, the model predicts a bit stronger northerly flow over eastern Wisconsin.

The narrow band of upward motion at 12 h (Fig. 14) extends farther north along the western shoreline than in the 4 January run. This is probably because the north-south temperature gradient between about 900 and 850 mb is considerably stronger in the 16 December case. As a result, the lapse rate between the lake surface and the air about 1 km above the surface is larger over the northern part of the lake. With the larger lapse rate, the PBL grows more rapidly and the vertical transfer of heat and moisture into the PBL is greater.

The predicted height of the PBL at 12 h (Fig. 15) is greatest over the western half of the lake. The height exceeds 1600 m along a nearly continuous band extending from the southern end of the lake into the far northern portion. At some grid points in the north, the PBL is predicted to grow more than 600 m higher in the 16 December simulation than in the 4 January run. This is consistent with the stronger mesoscale circulation over the northern part of the lake in the 16 December case.

The only precipitation predicted during the 12 h simulation is near the western shoreline, and the maximum amount is just under 2 mm. The predicted precipitation is more uniformly distributed along the band of upward motion than in the 4 January experiment.

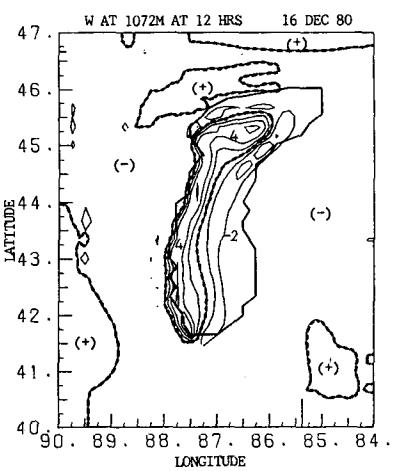

FIG. 14. As in Fig. 10 except for 16 December 1980 simulation.

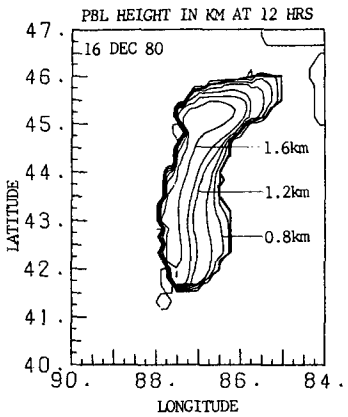

FIG. 15. As in Fig. 11 except for 16 December 1980 simulation.

5. Discussion

The model simulations indicate that the shoreline-parallel snowbands which occur with an easterly large-scale flow over Lake Michigan are part of a mesoscale land breeze circulation which develops when cold air below about 850 mb passes over the relatively warm lake surface and is heated from below. The circulation is characterized by a narrow band of upward motion along the western shoreline which results from the low-level convergence of easterly winds over the lake and north to northwesterly winds over land near the shore (the land breeze). An anticyclone north of Lake Michigan pushes an abundant supply of cold air westward across the lake where large quantities of heat and moisture are transported into a growing planetary boundary layer which reaches its maximum height near the western shoreline. Evidently, much of the moisture evaporated from the lake condenses in the vicinity of the land breeze convergence zone resulting in a persistent, nearly stationary band of precipitation (the snowband) parallel to the western shoreline. Radar observations of Passarelli and Braham (1981) indicate that these snowbands may consist of discrete cores of heavier precipitation, embedded within the more uniform precipitation, which tend to move slowly in a direction parallel to the axis of the band resulting in very little movement of the band itself.

There are similarities between the land-breeze-induced Lake Michigan snowband circulation and the coastal frontogenesis that occurs along the east coast of the United States. Both take place in late fall and early winter under large-scale easterly flow over relatively warm water, and both result in a narrow band of enhanced precipitation parallel to the coast. Ballentine (1980) concluded that the coastal convergence in New England coastal frontogenesis is due primarily to heat fluxes from the ocean and latent heat release.

The experiments suggest that the relative importance of latent heat release is even greater in the Lake Michigan snowband circulation. The magnitude of the upward motion and precipitation enhancement is considerably greater with coastal frontogenesis, since the Atlantic Ocean is a much greater heat source than Lake Michigan.

An important factor in the development of the lake snowband circulation is the temperature difference between the lake surface and the air over the lake up to about 850 mb. When this difference is sufficiently great, the rapid growth of the PBL permits a large quantity of heat and moisture to be transported into the atmosphere from the lake surface. Comparative experiments indicate that the strength of the mesoscale snowband circulation is approximately proportional to the temperature difference between the lake surface and the air at 850 mb. Another significant factor is the strength of the large-scale flow. When the easterly gradient over the lake is too strong, the land breeze circulation is unable to establish itself and shoreline parallel snowbands do not develop. In this case, if the air at 850 mb is sufficiently cold, snow squalls may form over Wisconsin many kilometers downwind from the lake. However, a strong easterly gradient is much more likely to be associated with the passage of a vigorous cyclone south of Lake Michigan, and pronounced warm advection at 850 mb reduces the temperature difference between the lake surface and the air above inhibiting the transfer of heat and moisture from the lake. When the easterly gradient is weak and the air–lake temperature difference is very large, an unusually well developed land breeze may push the snowband so far offshore that no snow is observed anywhere over land.

In forecasting the type of shoreline-parallel snowband described in this paper, the key element to watch for is a weak-to-moderate east to northeasterly flow set up by a *cold* anticyclone to the north of Lake Michigan. When a cyclone is moving eastward to the south of the lake, these snowbands are most likely to form when the circulation around the low is relatively weak.

Acknowledgments. The author expresses his thanks to meteorologists at the National Weather Service Office at Milwaukee's Mitchell Field for helpful discussions concerning the land-breeze-induced snowbands and for supplying data for a case study. He also wishes to thank Ms. Donna Bobst for typing the manuscript.

APPENDIX

List of Symbols

A constant $[=\exp(1/B) - 1]$
B constant $[=0.292]$
c^* phase speed of wave modes
D $[=\partial r/\partial z]$
E terrain elevation
H height of top of model
q specific humidity
r terrain following vertical coordinate
$\dot{r}$ vertical velocity component
θ potential temperature
Π Exner function $[=c_p(p/1000)^{R/c_p}]$.

REFERENCES

Asai, T., 1965: A numerical study of the air-mass transformation over Japan Sea in winter. *J. Meteor. Soc. Japan*, **43**, 1–15.

Ballentine, R., 1980: A numerical investigation of New England coastal frontogenesis. *Mon. Wea. Rev.*, **108**, 1479–1497.

Barnes, S., 1964: A technique for maximizing details in numerical weather map analysis. *J. Appl. Meteor.*, **3**, 396–409.

Deardorff, J. W., 1972: Parameterization of the planetary boundary layer for use in general circulation models. *Mon. Wea. Rev.*, **100**, 93–106.

——, 1974: Three-dimensional numerical study of the height and mean structure of a heated planetary boundary layer. *Bound.-Layer Meteor.*, **7**, 81–106.

Klemp, J. B., and D. K. Lilly, 1978: Numerical simulation of hydrostatic mountain waves. *J. Atmos. Sci.*, **35**, 78–107.

Passarelli, R., and R. Braham, 1981: The role of the winter land breeze in the formation of Great Lakes snowstorms. *Bull. Amer. Meteor. Soc.*, **62**, 482–491.

Pielke, R. A., and Y. Mahrer, 1975: Representation of the heated planetary boundary layer in mesoscale models with coarse vertical resolution. *J. Atmos. Sci.*, **32**, 2288–2308.